Journal of The Electrochemical Society, **158** (12) A1307-A1312 (2011)
0013-4651/2011/158(12)/A1307/6/$28.00 © The Electrochemical Society

Electrochemical Properties of Monoclinic $NaMnO_2$

Xiaohua Ma, Hailong Chen,* and Gerbrand Ceder,z**

Department of Materials Science and Engineering, Massachusetts Institute of Technology, Cambridge, Massachusetts 02139, USA

Monoclinic α- $NaMnO_2$ is re-investigated electrochemically as a positive electrode material for sodium ion batteries. About 0.85 Na can be deintercalated from $NaMnO_2$ and 0.8 Na be intercalated back during potentiostatical intermittent charge and discharge. Galvanostatical cycling between 2.0 V and 3.8 V gives 185 mAh/g discharge capacity for the first cycle at C/10 rate and 132 mAh/g remains after 20 cycles. Charge and discharge curves are significantly different indicating more hysteresis than is typical for lithium intercalation compounds. We also explain the remarkable difference between layered $LiMnO_2$ and $NaMnO_2$ upon alkali removal.
 [DOI: 10.1149/2.035112jes]

Manuscript submitted June 24, 2011; revised manuscript received September 2, 2011. Published October 31, 2011.

Li_xMO_2 (M = 3d transition metal) compounds with the O3 layered structure have been intensively studied as positive electrode materials for lithium ion batteries, and $LiCoO_2$ and $LiNiO_2$ –based materials operate well as Li-intercalation materials. For several other 3*d* transition metals $LiMO_2$ either does not easily form the O3-layered structure (M = Ti, Fe, Mn), or does not reversibly deintercalate lithium (M = V, Cr, Fe, Mn).[1–3] Indeed, layered $LiFeO_2$ and $LiMnO_2$ can only be obtained from their Na phase by Li/Na ion exchange[3–5] but $LiFeO_2$ does not deintercalate lithium well,[6,7] and $LiMnO_2$ transforms to spinel in the first charge or discharge [8] due to the high mobility of Mn^{2+}.[9,10] This situation is in sharp contrast to the $NaMO_2$ compounds. Na_xMO_2 systems form layered structures more easily due to the larger ionic size difference between alkaline and transition metals.[11,12] The deintercalation and intercalation of sodium in layered Na_xMO_2 has been reported for M = Ti, V, Cr, Mn, Fe, Co, Ni.[2,13–20] Furthermore, several Na compounds with mixed transition metals, having either tunnel or layered structures, such as $Na_xNi_{0.6}Co_{0.4}O_2$, $Na_xNi_yMn_{1-y}O_2$, $Na_xTi_yMn_{1-y}O_2$, have also been studied as positive electrode materials.[21–25] In this paper we focus on the layered $NaMnO_2$ as a possible Na-intercalation cathode, and show that unlike $LiMnO_2$, a large amount of alkali ions can be reversibly cycled from $NaMnO_2$.

The known phases of Na_xMnO_2 ($x = 0.2, 0.40, 0.44, 0.70, 1$) have been summarized by Parant, et al.[26] There are two phases for $NaMnO_2$. Low temperature α- $NaMnO_2$ has an O3 layered structure with a monoclinic structural distortion due to the Jahn-Teller distortion of the Mn^{3+} ion. At high temperature, the orthorhombic β- $NaMnO_2$ forms in a different layered structure containing MnO_2 sheets consisting of a double stack of edge-sharing MnO_6 octahedra. Na occupies the octahedral sites between two neighboring sheets.[17] First principles computations indicate that the monoclinic $NaMnO_2$ is energetically more stable than other competing phases.[27] This is in contrast to $LiMnO_2$, which prefers an orthorhombic structure.[27,28]

Both α- and β- $NaMnO_2$ have been electrochemically tested as a positive electrode material by Mendiboure, et al. in 1985. Their results showed that only 0.22 and 0.15 Na could be reversibly extracted and re-intercalated in α- and β- $NaMnO_2$ respectively. Besides $NaMnO_2$, $Na_{0.4}MnO_2$, $Na_{0.6}MnO_2$, $Na_{0.7}MnO_{2.25}$ have also been studied as a positive electrode in sodium ion batteries.[17,29] Among them, P2-$Na_{0.6}MnO_2$ shows the highest capacity of about 150 mAh/g at the first cycle. The capacity decays to about 70 mAh/g over 10 cycles.[29]

In this paper, we report on the synthesis and electrochemical testing of monoclinic α- $NaMnO_2$. Our results show, in contrast to previous work, that 0.85 Na can be deintercalated and 0.8 Na intercalated back reversibly, corresponding to 210 mAh/g charge capacity and 197 mAh/g discharge capacity. We also show reasonable capacity retention with galvanostatic cycling.

Experimental Methods

$NaMnO_2$ was synthesized by solid-state reaction. Stoichiometric amounts of $NaCO_3$ (100%, Baker) and Mn_2O_3 (98%, Alfa Aesar) were mixed and ball milled in aceton for 6 hours at 300 rpm rate. The mixture was dried into a powder. About 0.5g of powder was pressed into a pellet. The pellet was fired at 700°C in air for 10 hours before it was quenched to room temperature and moved to a glove box filled with argon.

X-ray diffraction (XRD) patterns were collected on a Rigaku Rotaflex or PANalytical X'pert pro diffractometer equipped with Cu Kα radiation in the 2θ range of 10–80°. All the samples were sealed with Kapton film to avoid air exposure. Rietveld refinement and profile matching of the powder diffraction data of the as-prepared $NaMnO_2$ were performed with Fullprof using space group C2/m.

The atomic ratio of Na and Mn in as-prepared $NaMnO_2$ powder was determined by direct current plasma (DCP) emission spectroscopy (Luvak Inc., Boylston, MA 01505). After cycling, the electrolyte and the Na metal anode were collected and analyzed for Mn content by ICP technique (HORIBA Jobin Yvon ACTIVA ICP-AES Spectrometer) to investigate potential Mn dissolution.

Electrochemical cells were configured in the following way: Na/ 1 M $NaPF_6$ in EC:DMC = 1:1/ $NaMnO_2$ with carbon black (15 wt%) as conductive agent and polyethylenetetrafluoride (PTFE) (5 wt%) as binder. The 1 M $NaPF_6$ in EC:DMC electrolyte was prepared by dissolving anhydrous $NaPF_6$ (98%, Sigma Aldrich) into EC:DMC (anhydrous, Sigma Aldrich, 1:1 in volume ratio). Two pieces of glass fiber served as separators and stainless steel as current collectors in Swagelok cells, assembled in an argon-filled glove box with the moisture level less than 0.1 ppm. The cells were cycled at room temperature using a Maccor 4000 operating in the galvanostatic mode.

The Na content vs. voltage was measured by potentiostatic intermittent titration (PITT) on a Solartron 1287 electrochemical potentiostat. Steps of 10 mV were taken to fully charge and discharge the cell. The capacity was measured at each voltage step until the current was below C/50.

Experimental Results

The XRD pattern of as-prepared monoclinic $NaMnO_2$ is shown in Fig. 1. The background and three broad peaks between 10–30° are from the Kapton film. Rietveld refinement gives the lattice parameters $a = 5.672$ Å, $b = 2.856$ Å, $c = 5.807$ Å, $\beta = 113.2°$. These values are fairly close to the results of Mendiboure, et al. ($a = 5.63$ Å, $b = 2.86$ Å, $c = 5.77$ Å, $\beta = 112.9°$).[4,17,26,30] The Mn-O bond lengths in the MnO_6 octahedron are 2.39 Å (2×) and 1.94 Å (4×) respectively, confirming that Mn^{3+} is Jahn-Teller active.[27,30]

The DCP data shows that the as-prepared $NaMnO_2$ consists of 20.5% Na and 49.1% Mn in weight, giving an atomic ratio of Na and Mn to be 1:1. Assuming that the as-prepared $NaMnO_2$ is 100%

* Electrochemical Society Student Member.
** Electrochemical Society Active Member.
z E-mail: gceder@mit.edu

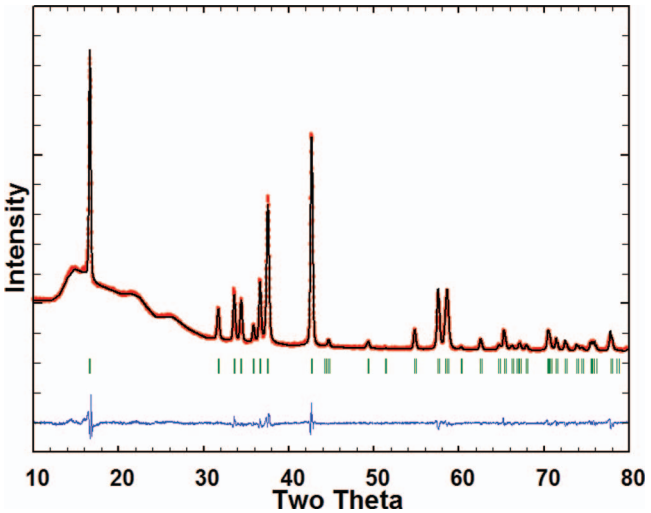

Figure 1. XRD pattern and refinement of as-prepared $NaMnO_2$. The broad peaks between 10° and 30° are due to the Kapton film used to seal the sample. The red (black) line represents the experimental (calculated) data. The residual discrepancy is shown in blue. The refinement results are preformed in the C2/m space group and give $R_{wp} = 10.2\%$, and $\chi^2 = 9.98$.

phase-pure and that the remainder 30.4% of the total weight is oxygen, the chemical formula can be determined as $NaMnO_{2.06}$.

Fig. 2 shows the capacity vs. voltage measured by PITT on the as-prepared $NaMnO_2$. Fig. 2a and 2b are for the 1st and 2nd PITT cycle respectively. The results were plotted in a manner resembling cyclic voltammograms except that the current is replaced by the capacity. The results show a series of peaks in both charge and discharge, indicating a multitude of possible phase transitions as the system is de-sodiated. In the 1st PITT cycle, the charge process consists of eight oxidation peaks set: 2.59 V, 2.63 V, 2.73 V, 2.80 V, 2.97 V, 3.14 V, 3.48 V and 3.59 V, while the discharge process consists of only five considerably less pronounced reduction peaks: 2.47 V, 2.62 V, 2.87 V, 3.08 V, 3.45 V. Similar differences between the charge and discharge profile were found in the sequential two PITT cycles with the same cell. In the 2nd and 3rd cycles, most peaks are at the same positions, except that two oxidation peaks at 2.59 V, 2.63 V are merged into one peak at 2.56 V and one new peak appears at 2.91 V (shown in Fig. 2b). The distinctly different charge and discharge peaks indicate that the charge and discharge process probably go through different reaction paths with different intermediate phases. However, this hysteresis seems to be reversible, given that the charge and discharge profile are largely preserved in the 2nd and 3rd cycle.

The data in Fig. 2 can also be represented in Fig. 3 where Na content is plotted vs. voltage. The Na content is calculated from adding the capacity at each voltage step in the PITT measurement. The initial Na content is 1 as determined by DCP. The series of plateaus in Fig. 3 correspond to the peaks in Fig. 2. The difference between charge and discharge can also be observed in the different charge/discharge voltage profiles. About 0.85 Na, corresponding to a charge capacity of 210 mAh/g, can be deintercalated from $NaMnO_2$ when the cell is charged up to 3.8 V vs. Na/Na^+ in PITT. Upon discharge to 2 V, 0.8 Na (corresponding to discharge capacity 197 mAh/g) can be reversibly intercalated back.

Fig. 4 shows the galvanostatic charge and discharge of $NaMnO_2$ at C/10 and C/30 at various cycles (1C = 240 mAh/g). At C/10, the charge/discharge capacities in the first and tenth cycle are 214/185 mAh/g and 165/149 mAh/g respectively. At C/30, 209/194 mAh/g is achieved in the first cycle and 207/144 mAh/g in the tenth cycle. The coulombic efficiencies are low at both C/10 and C/30 rate (C/10: 86.4% for first cycle, 90.3% for tenth cycle; C/30: 92.8% for first cycle, 70% for tenth cycle). The low coulombic efficiency implies that side reactions, possibly with the electrolyte,

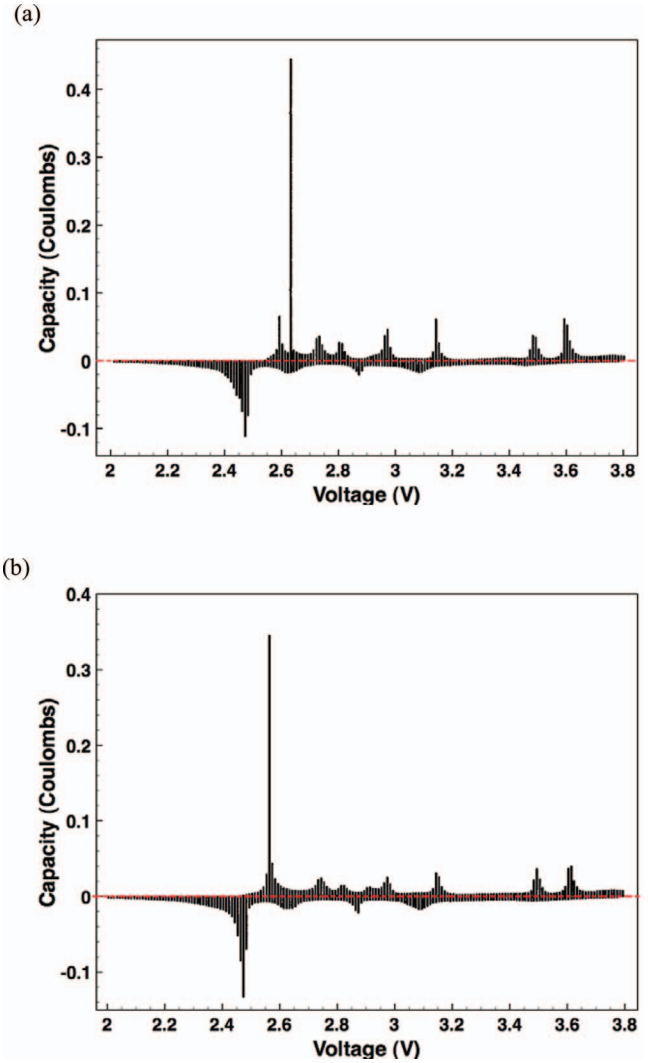

Figure 2. Capacity vs voltage of Na deintercalation (upper) and intercalation (lower) for $NaMnO_2$ measured by PITT with 10mV steps. (a) is for the first cycle and (b) for the second cycle.

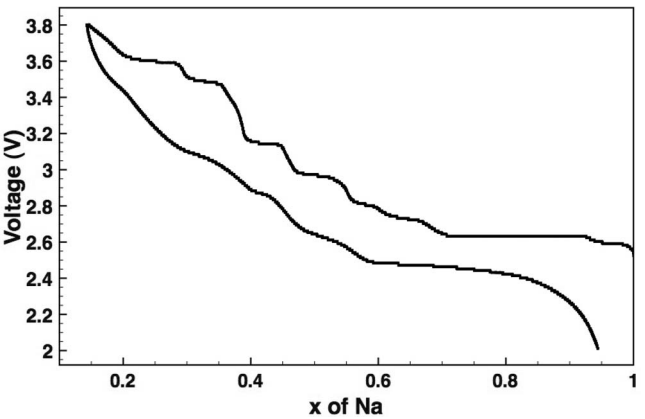

Figure 3. Voltage profile of Na_xMnO_2 upon Na deintercalation and intercalation measured by PITT. The cell is potentiostatically charged up to 3.8 V vs Na/Na^+ and discharged to 2.0 V.

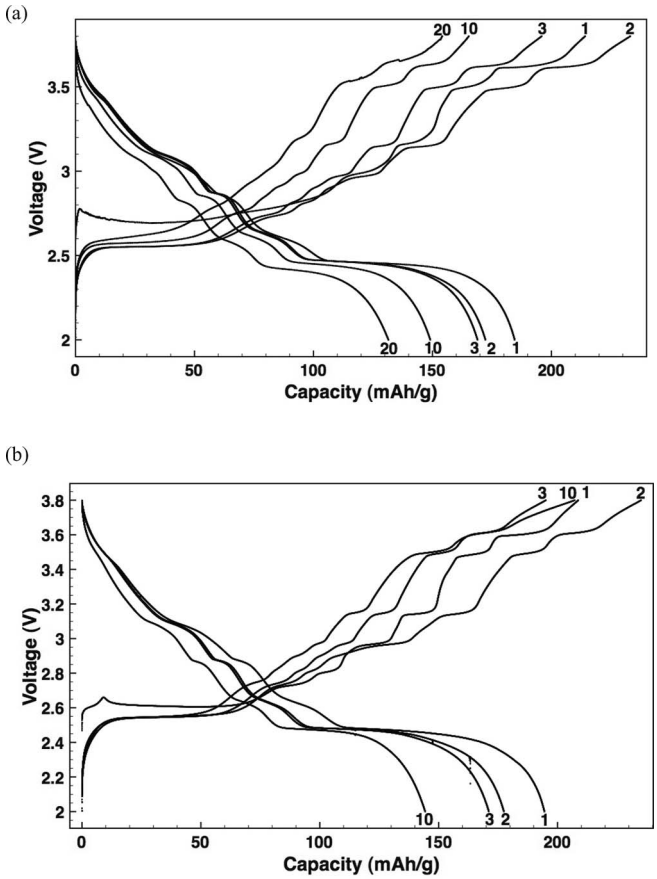

Figure 4. Voltage profile of $NaMnO_2$ after multiple cycles at C/10 (a) and C/30 (b) respectively. The cell is galvanostatically cycled between 2.0 V and 3.8 V.

take place during charge, especially at higher voltage. When testing with a C/30 rate, the cell experiences high voltage for longer time, causing more parasitic reaction and/or degradation, hence the lower Coulombic efficiency. It is not clear from our data whether the poor Coulombic efficiency is the result of materials degradation, or due to a self-discharge shuttle in the electrolyte. Fig. 5 compares the voltage profiles of $NaMnO_2$ charged up to 3.8 V and 4.2 V respectively. When the cell is charged up to 4.2 V, it shows an additional charge capacity

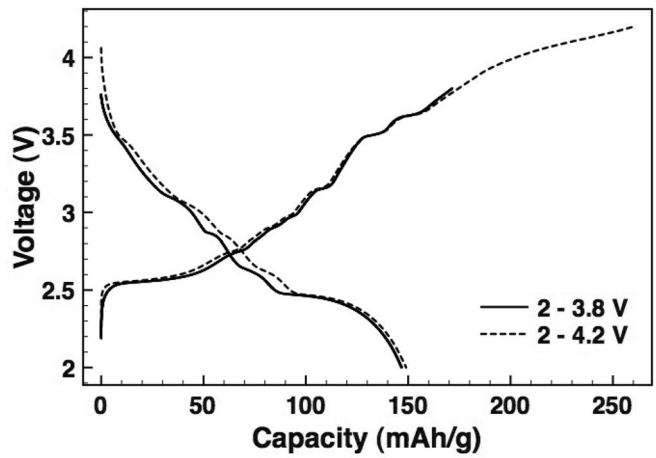

Figure 5. Comparison of the voltage profiles of $NaMnO_2$ charged up to 3.8 V and 4.2 V respectively. The cell was galvanostatically cycled at C/10 rate.

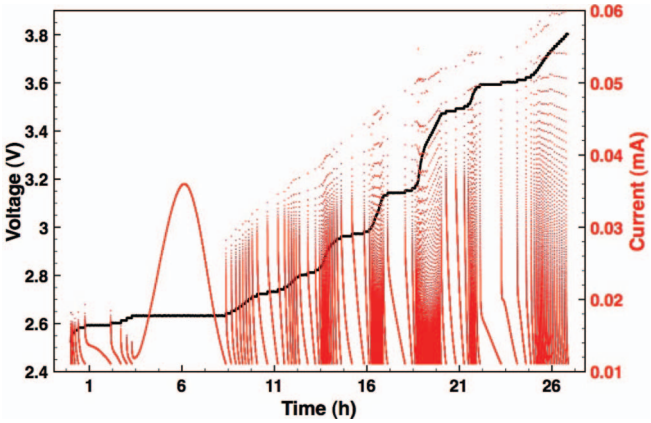

Figure 6. Voltage steps (black) and the corresponding current relaxation (red) during PITT measurements in the first charge cycle.

of about 90 mAh/g between 3.8 V and 4.2 V. However, this additional capacity is not shown during discharge, indicating the charge capacity between 3.8 V and 4.2 V is mainly from the decomposition of the electrolyte. On the other hand, the $NaMnO_2$ electrode material does not seem to be significantly affected by the overcharge as the discharge profiles after charging up to 3.8 V and 4.2 V are very similar.

We have investigated the long voltage plateau at 2.63 V, starting from $\approx Na_{0.93}MnO_2$ and ending at $\approx Na_{0.70}MnO_2$. In Fig. 6 we show the result of current relaxations after 10 mV voltage steps. In the voltage plateau region the current is initially low after a small potential step, but then slowly ramps up to its maximum after about 2.5 hours. This current behavior is typical of a two-phase reaction with a significant phase transformation barrier (i.e. a first order phase transition).[31] Initially, the current is low as nucleation needs to occur, but once nucleation starts the current increases significantly as the second phase grows. The first charge in Fig. 4 also shows the typical voltage overshoot at both C/10 and C/30, typically associated with the onset of a first order phase transformation.

To confirm the two-phase reaction, ex situ XRD analysis was performed on an electrode that was removed from a cell, which was charged to the middle of the plateau (nominal Na content about 0.83). Fig. 7 compares the XRD pattern of the charged electrode $Na_{0.83}MnO_2$ to that of uncharged $NaMnO_2$. The results confirm the two-phase coexistence: One phase in the XRD of the partially charged cathode material matches with pristine $NaMnO_2$ with very little peak shift. From Fig. 3, we estimate the composition of this phase to be $\approx Na_{0.93}MnO_2$. The lattice parameters of the $Na_{0.93}MnO_2$ phase are $a = 5.671$ Å, $b = 2.817$ Å, $c = 5.806$ Å, $\beta = 113.2^\circ$, as obtained by fitting the diffraction pattern. All the values are almost identical to those of the pristine $NaMnO_2$ except that the b–lattice parameter has contracted by 1.4%. From the charge/discharge curve in Fig. 3, we estimate that the composition of the second phase in the XRD pattern of the partially charged material, is $\approx Na_{0.70}MnO_2$. The $Na_{0.70}MnO_2$ phase is indexed in Fig. 7 on a monoclinic lattice. The lattice parameters of this $Na_{0.70}MnO_2$ phase are shown in Table I. In layered Na_xMnO_2, Na and Mn are ordered in alternative (111) planes of an FCC cubic

Table I. Comparison of lattice parameters of $Na_{0.93}MnO_2$ and $Na_{0.70}MnO_2$.

Samples	$Na_{0.93}MnO_2$	$Na_{0.70}MnO_2$	Misfit (%)
a (Å)	5.671	5.126	9.6
b (Å)	2.817	2.921	3.7
c (Å)	16.054	16.737	4.3
β (°)	94.25	91.82	2.6
Volume (Å^3)	255.76	250.50	2.1

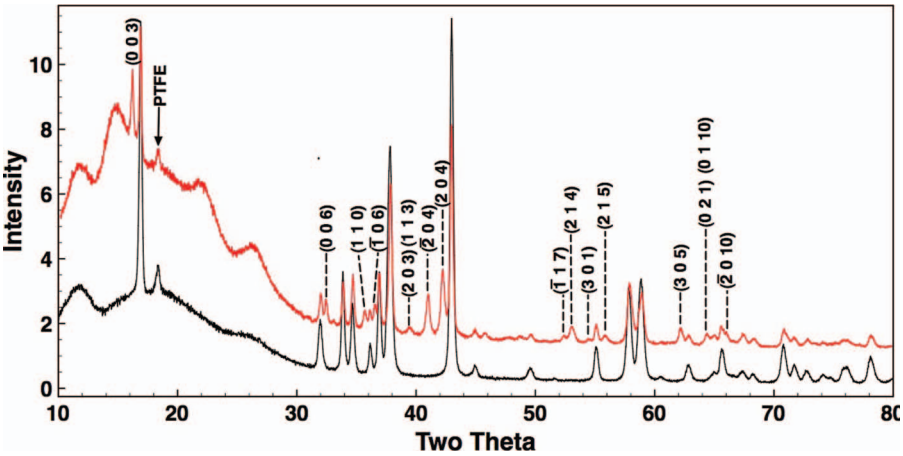

Figure 7. XRD of fresh $NaMnO_2$ electrode (black) and partially charged $Na_{0.83}MnO_2$ (red). New peaks corresponding to $Na_{0.70}MnO_2$ are indexed using a monoclinic lattice.

close-packed oxygen framework. The monoclinic cell used for the $Na_{0.70}MnO_2$ phase, contains six metal layers, contrary to two layers in the $Na_{0.93}MnO_2$ phase. This cell tripling can be due to the Na/vacancy ordering (both in-plane and inter-plane) that lowers the symmetry or to oxygen layer gliding to modify the O3-stacking.[32] To compare the lattice parameters of the coexisting two phases, we use the tripled unit cell for $Na_{0.93}MnO_2$ as indicated by the dashed lines in Fig. 8.

Table I compares the lattice parameters of $Na_{0.70}MnO_2$ and $Na_{0.93}MnO_2$ in the same supercell setting. The changes in lattice constants upon Na removal are significant, with a reduced by 9.6% and b and c increasing. The angle β also changes by 2.6%. The significant lattice misfit implies considerable strain between the two phases, which could be responsible for the significant phase transformation barrier observed in the current relaxation data in Fig. 6.

It has been reported that chemically synthesized $Na_{0.70}MnO_2$ usually exhibits some transition metal vacancies (equivalent to oxygen over-stoichiometry),[33] so the compound is usually written as $Na_{0.70}MnO_{2+y}$ ($0 < y < 0.25$). There are two known structures reported for $Na_{0.70}MnO_{2+y}$ depending on the amount of excess oxygen.[26,33] One is orthorhombic with space group Cmcm (for $0 < y < 0.05$) and the other hexagonal with space group $P6_3/mmc$ (for $0.05 < y < 0.25$). The XRD pattern of the $Na_{0.70}MnO_2$ phase we obtained by electrochemical deintercalation, however, does not match either of the above two phases. Its diffraction pattern is actually quite similar to that of $Na_{0.74}CrO_2$ whose structure is unsolved as of yet.[34]

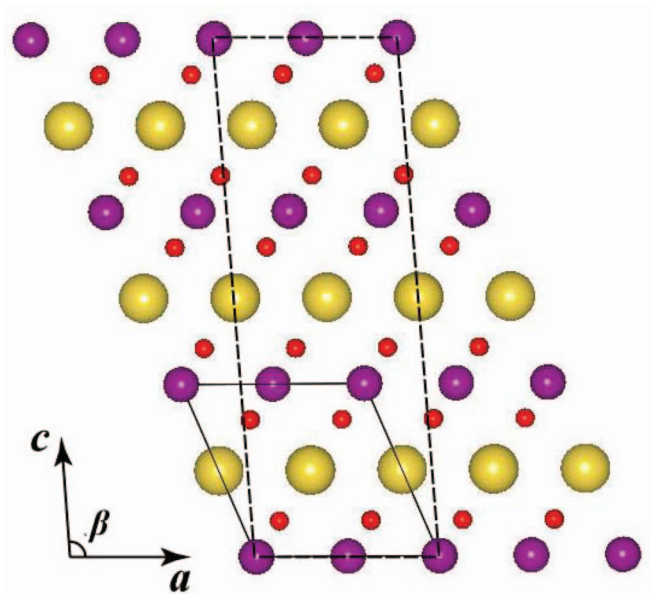

Figure 8. Structure of monoclinic $Na_{0.93}MnO_2$ projected in a-c plane. (purple - Mn, yellow – Na, red - Oxygen) The solid line indicates the unit cell of monoclinic $Na_{0.93}MnO_2$. The super cell indicated by the dashed line is more comparable to the unit cell of the $Na_{0.70}MnO_2$ phase.

Some capacity decline with cycling is evident from Fig. 4. The relative decay of discharge capacity is more severe at C/30 rate than that at C/10. To investigate the reason for the capacity decay, a cell cycled for 20 cycles was dismantled in the discharged state, and the cathode electrode washed in anhydrous DMC in an argon filled glove box for XRD. Fig. 9 compares the XRD patterns of the cycled and fresh electrodes. The two patterns are very similar, but the peaks after cycling become broadened. Rietveld refinement results from the cycled electrode gives lattice parameters: $a = 5.654$ Å, $b = 2.861$ Å, $c = 5.808$ Å, $\beta = 112.97°$, less than 0.3% different from the refinement results of pristine $NaMnO_2$. In the peak shape refinement, the Gaussian composition of the peak broadening does not change after cycling but the Lorentzian composition increases. The related parameters are $x = 0.247$, $y = 0.073$ in the fresh electrode and $x = 0.159$, $y = 0.257$ in the cycled electrode respectively. The Gaussian broadening x is typically related to crystal strain, while y is related to crystal size and faulting.[35] In the cycled electrode, x is decreased implying less crystal strain. The increase of y parameter indicates that either the crystal size decreased, or more likely, that more faulting occurred.

With Mn^{3+} containing cathode materials, possible dissolution of Mn due to its disproportionation to Mn^{2+}, is always a cause of concern.[36] To find out how much Mn is dissolved into the electrolyte or deposited on the Na anode surface after cycling, the electrolyte from the cycled cell (20 cycles at C/10 rate with a total soaking time of ~270 hours) and the Na anode surface were collected for analysis. The electrolyte was diluted into water, and the surface of the Na anode was also scraped and dissolved into water to form a dilute solution. The diluted solutions were analyzed by ICP to measure the concentration of Na and Mn. In the data analysis of the electrolyte, the Na concentration was used as a reference since the Na concentration in the undiluted electrolyte is known as 1 mol/*l*. For the surface of the Na anode, the total weight of the dilute solution was measured to estimate the amount of the possible Mn deposition. Table II shows the Na and

Table II. Summary of ICP results of Na anode surface, fresh and cycled electrolyte in the water diluted solution.

Samples	Na (ppm)	Mn (ppm)
Fresh electrolyte	361	~0
Cycled electrolyte	145	<0.2
Na anode surface	701	~0

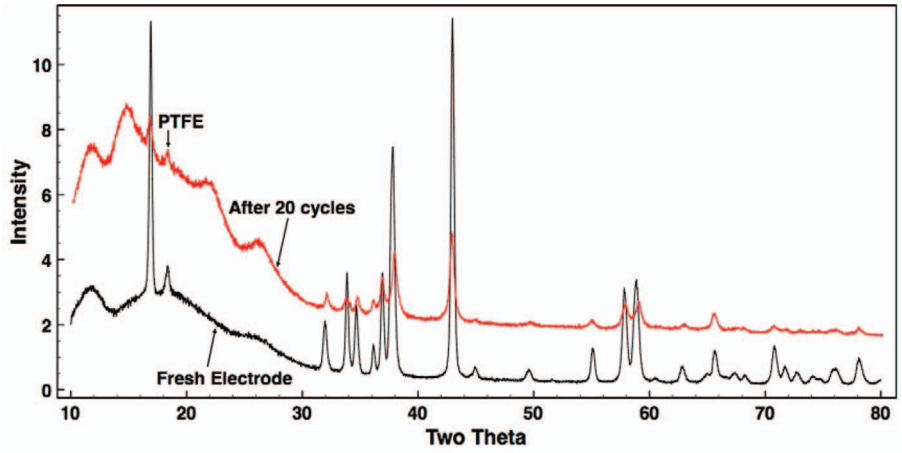

Figure 9. XRD patterns of fresh electrode (black) and cycled electrode (red).

Mn concentration in the diluted solutions. The Mn concentration in the fresh electrolyte and on the fresh Na anode surface is negligible. In the diluted solution of the cycled electrolyte, the concentration of Mn is less than 0.2 ppm. As the Na concentration in undiluted electrolyte is known as 1mol/*l* ($\sim 23 \times 10^3$ ppm), we can estimate the concentration of Mn in undiluted cycled electrolyte to be less than 32 ppm. In our cell the electrolyte is less than 1 *ml*, therefore the amount of Mn dissolved in the electrolyte is less than 32 μg. The typical cathode weight in our cell is about 2–3 mg. Therefore, only a few percent of Mn is dissolved, which is unlikely to cause the significant capacity decay we observed. It should however not be excluded that dissolved Mn can be deposited on other cell components, such as in the separator.

It is also possible that impedance increase at the sodium/electrolyte interface leads to apparent capacity fade. The increased overpotential would lead to a premature charge cutoff as the voltage limit is fixed in experiments, resulting in an apparent capacity fade. The voltage profile in Fig. 4 lends support to this possibility, as overpotentials for both the charge and discharge processes increase over cycling.

Discussion

We achieve a very high charge and discharge capacity from monoclinic $NaMnO_2$ with the O3 structure. Our results are significantly better than those obtained by Mendiboure, et al., who evaluated monoclinic $NaMnO_2$ with 1 M $NaClO_4$ in PC as electrolyte.[17] Their open circuit voltage curve shows a voltage plateau around 2.7 V ranging from $Na_{0.93}MnO_2$ to $Na_{0.73}MnO_2$, which is close to the plateau we observe at 2.63 V. However, only about 0.22 Na could be deintercalated/intercalated from $NaMnO_2$ in their work, and no obvious voltage plateau appeared in their study. In our results, about 0.7 Na can be deintercalated up to a charge cutoff of 3.5 V. The reasons for this difference are not clear though they may be related to the difference in electrolyte used.

The voltage versus capacity shows very pronounced features with strong voltage steps and plateaus indicative of phase transitions upon desodiation. Such strong features have also been observed for intercalation of Na in $NaCoO_2$,[37] but are less common in Li-intercalation systems unless structural or electronic transitions [38] are involved. The phase changes in Na_xMnO_2 can be due to Na-vacancy ordering or transitions that involve the gliding of oxygen planes. The latter is a possibility in Na-deintercalation reactions as Na prefers both octahedral and trigonal prismatic environments and the trigonal prismatic coordination can only be achieved in an O3 stacking by sliding some of the oxygen layers.[13]

Careful inspection of Fig. 3 and 4 indicates that the sequence of phase transformation on charge and discharge is not the same. This is consistent with the strong first order character of the phase transformations. When the two phases on each side of the transition are very distinct, nucleation is often not symmetric. This is similar to the asymmetry between the melting and solidification transition of solids. At this point we do not understand why transitions in Na_xMnO_2 are so pronounced. It is possible that Na-vacancy ordering interactions are stronger than for Li-vacancy due to the larger size of Na, which would add large elastic contributions to the screened electrostatic interactions between the alkali and the vacancy.[39] Another likely possibility is the occurrence of structural transitions, which affect the oxygen stacking. Such oxygen layer gliding would modify the Na coordination and allow it to be optimized at each Na concentrations. In each case, the strong phase transitions in Na-intercalation oxides may create more hysteresis and reduce the energy efficiency, similar to the problems with conversion reactions in lithium systems.[40]

Several other $NaMO_2$ (M = V, Cr, Fe) oxides have been evaluated as intercalation cathodes. While $NaMO_2$ (M = V, Cr, Fe) can be reversibly cycled up to $Na_{0.5}MO_2$, only a very small amount of Na can be intercalated back when these materials are further charged.[19,20,25] However, $NaMnO_2$ can be deintercalated up to $Na_{0.15}MnO_2$ with 0.8 Na being reversibly intercalated back. Secondly, for $NaMO_2$ (M = V, Cr, Fe) the reversibility is improved with lower charge cutoff voltage,[19,20,25] but for $NaMnO_2$ the cyclability becomes worse when the charge voltage is lowered from 3.8 V to 3.4 V, as is shown in Fig. 10.

It is instructive to compare the remarkable difference in the electrochemical behavior of $NaMnO_2$ with that of $LiMnO_2$. Layered $LiMnO_2$ can be obtained from $NaMnO_2$ by ion exchange. During cycling of $LiMnO_2$, the capacity decays rapidly and the structure becomes

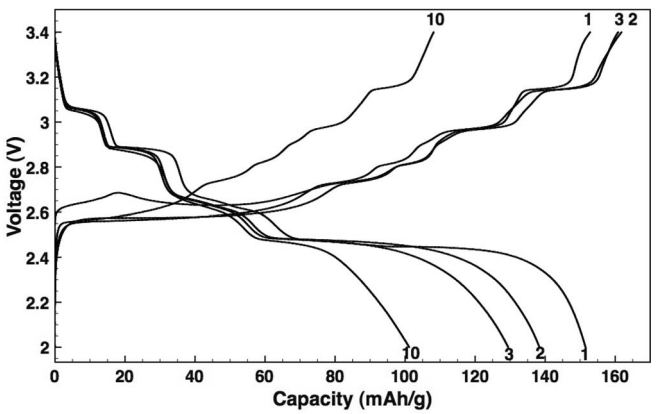

Figure 10. Cyclability of $NaMnO_2$ at lower cutoff voltage. The cell is cycled at C/10 within voltage window 2–3.4 V.

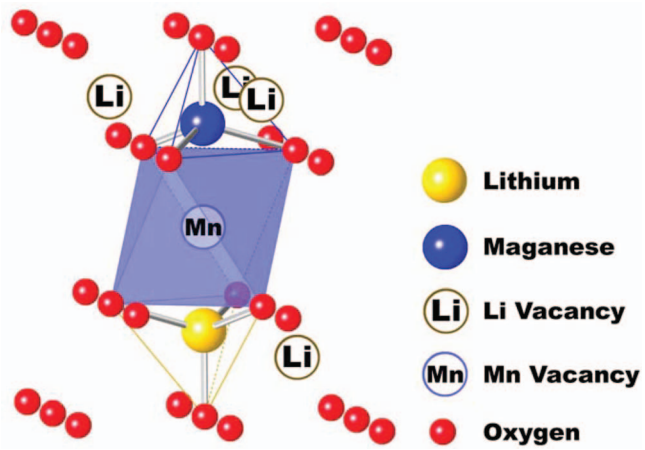

Figure 11. Demonstration of the Li/Mn dumbbell configuration in layered $LiMnO_2$. Mn migrates to the tetrahedral site in Li layer leaving a Mn vacancy in Mn layer. Li trivacancy is necessary to avoid face sharing with Mn.

spinel-like.[8] The transformation from layered to spinel requires the migration of Mn ions from the transition metal layer into the alkali layer. It is clear from comparing the electrochemical behavior of O3-$LiMnO_2$ to O3-$NaMnO_2$ that the alkali plays a critical role in this migration. Removing the alkali from both compounds leads to the same structures, but the $LiMnO_2$ system transforms to spinel while $NaMnO_2$ does not. This difference in behavior is consistent with the model proposed by Reed, et al. using first principles computation.[10] Reed, et al. argued that in $LiMnO_2$, Mn can migrate into tetrahedral sites when trivacancies are formed in the Li layer. Meanwhile, a Li ion can move to a tetrahedral site in the adjacent Li layer to form the Li/Mn dumbbell configuration as is shown in Fig. 11. This type of dumbbell configuration can stabilize the Mn in tetrahedral sites and serves as nucleus for the layered to spinel phase transformation. It was pointed out that Mn in a tetrahedral site without an accompanying Li in a tetrahedral site was actually unstable energetically.[41] In $NaMnO_2$, however, Na is unlikely to move to a tetrahedral site and can therefore not stabilize Mn in a tetrahedral site. Hence, with Na, the intermediate state in the transformation of layered to spinel is not stable giving the layered Na_xMnO_2 good metastability, thereby resulting in good cyclability of the material. In addition, driving force to transform from the layered to the spinel structure is also reduced, as spinels with Na in the tetrahedral sites are much less common due to the size difference between Na and 3d transition metals such as Mn.

Conclusion

Monoclinic $NaMnO_2$ is synthesized and tested electrochemically as a positive electrode material for a sodium ion battery. About 0.85 Na can be deintercalated out of $NaMnO_2$ and 0.8 Na can be reversibly intercalated back. The charge and discharge profile show a different series of plateaus indicating different reaction paths with different intermediate phases. Current relaxation in PITT indicates a phase transformation barrier at the 2.63 V plateau, which was confirmed to be a two-phase reaction by XRD. While some capacity fade was observed after 20 cycles, no significant structural change was found after cycling. From our results it is clear that cyclability of corresponding Na and Li compounds can be very different.

Acknowledgments

This work made use of the Shared Experimental Facilities supported in part by the MRSEC Program of the National Science Foundation under award number DMR – 0819762. We also acknowledge the Office of Naval Research Sponsor Award N00014-11-1-0212 for financial support. We thank Dr. Byoungwoo Kang and Dr. Qing Hao for fruitful discussions.

References

1. L. Zhang, K. Takada, N. Ohta, M. Osada, and T. Sasaki, *J. Power Sources*, **174**, 1007 (2007).
2. S. Komaba, C. Takei, T. Nakayama, A. Ogata, and N. Yabuuchi, *Electrochem. Comm.*, **12**, 355 (2010).
3. A. R. Armstrong and P. G. Bruce, *Nature*, **381**, 499 (1996).
4. B. Fuchs and S. Kemmler-Sack, *Solid State Ionics*, **68**, 279 (1994).
5. T. Shirane, R. Kanno, Y. Kawamoto, Y. Takeda, M. Takano, T. Kamiyama, and F. Izumi, *Solid State Ionics*, **79**, 227 (1995).
6. M. Tabuchi, C. Masquelier, T. Takeuchi, K. Ado, I. Matsubara, T. Shirane, R. Kanno, S. Tsutsui, S. Nasu, H. Sakaebe, and O. Nakamura, *Solid State Ionics*, **90**, 129 (1996).
7. J. Li, J. Li, J. Luo, L. Wang, and X. He, *Int. J. Electrochem. Sci.*, **6**, 1550 (2011).
8. Y. Shao-Horn, S. A. Hackney, A. R. Amstrong, P. G. Bruce, R. Gitzendanner, C. S. Johnson, and M. M. Thackeray, *J. Electrochem. Soc.*, **146**, 2404 (1999).
9. J. Reed, G. Ceder, and A. Van der Ven, *Electrochem. Solid-State Lett.*, **4**, A78 (2001).
10. J. Reed and G. Ceder, *Chem. Rev.*, **104**, 4513 (2004).
11. E. J. Wu, P. D. Tepesch, and G. Ceder, *Philos. Mag. B*, **77**, 1039 (1998).
12. T. A. Hewston and B. L. Chamberland, *J. Phys. Chem. Solids*, **48**, 97 (1987).
13. C. Delmas, J. J. Braconnier, C. Fouassier, and P. Hagenmuller, *Solid State Ionics*, **3**, 165 (1981).
14. J. J. Braconnier, C. Delmas, and P. Hagenmuller, *Mat. Res. Bull.*, **17**, 993 (1982).
15. A. Maazaz, C. Delmas, and P. Hagenmuller, *J. Inclusion Phenom.*, **1**, 45 (1983).
16. S. Kikkawa, S. Miyazaki, and M. Koizumi, *J. Power Sources*, **14**, 231 (1985).
17. A. Mendiboure, C. Delmas, and P. Hagenmuller, *J. Solid State Chem.*, **57**, 323 (1985).
18. L. W. Shacklette, T. R. Jow, and L. Townsend, *J. Electrochem. Soc.*, **135**, 2669 (1988).
19. Y. Takeda, K. Nakahara, M. Nishijima, N. Imanishi, O. Yamamoto, M. Takano, and R. Kanno, *Mat. Res. Bull.*, **29**, 659 (1994).
20. C. Didier, M. Guignard, C. Denage, O. Szajwaj, S. Ito, I. Saadoune, J. Darriet, and C. Delmas, *Electrochem. Solid-State Lett.*, **14**, A75 (2011).
21. I. Saadoune, A. Maazaz, M. Menetrier, and C. Delmas, *J. Solid State Chem.*, **122**, 111 (1996).
22. J. M. Paulsen and J. R. Dahn, *Solid State Ionics*, **126**, 3 (1999).
23. Z. Lu and J. R. Dahn, *J. Electrochem. Soc.*, **148**, A1225 (2001).
24. M. M. Doeff, T. J. Richardson, and K. T. Hwang, *J. Power Sources*, **135**, 240 (2004).
25. S. Komaba, T. Nakayama, A. Ogata, T. Shimizu, C. Takei, S. Takada, A. Hokura, and I. Nakai, *ECS Trans.*, **16**, 43 (2009).
26. J. P. Parant, R. Olazcuaga, M. Devalette, C. Fouassier, and E. T. P. Hagenmuller, *J. Solid State Chem.*, **3**, 1 (1971).
27. O. I. Velikokhatnyi, C.-C. Chang, and P. N. Kumta, *J. Electrochem. Soc.*, **150**, A1262 (2003).
28. R. Hoppe, G. Brachtel, and M. Jansen, *Z. Anorg. Allg. Chem.*, **417**, 1 (1975).
29. A. Caballero, L. Hernán, J. Morales, L. Sánchez, J. Santos Peña, and M. A. G. Aranda, *J. Mater. Chem.*, **12**, 1142 (2002).
30. M. Jansen and R. Hoppe, *Z. Anorg. Allg. Chem.*, **399**, 163 (1973).
31. N. Meethong, H-Y. S. Huang, S. A. Speakman, W. C. Carter, and Y-M. Chiang, *Adv. Funct. Mater.*, **17**, 1115 (2007).
32. Y. Hinuma, Y. Meng, and G. Ceder, *Phys. Rev. B*, **77**, 1 (2008).
33. R. Stoyanova, D. Carlier, M. Sendova-Vassileva, M. Yoncheva, E. Zhecheva, D. Nihtianova, and C. Delmas, *J. Solid State Chem.*, **183**, 1372 (2010).
34. S. Miyazaki, S. Kikkawa, and M. Koizumi, *Rev. Chim. Miner.*, **19**, 301 (1982).
35. R. J. Hill, *Advances in X-Ray Analysis*, **35**, 25 (1992).
36. Y. Terada, Y. Nishiwaki, I. Nakai, and F. Nishikawa, *J. Power Sources*, **97–98**, 420 (2001).
37. R. Berthelot, D. Carlier, and C. Delmas, *Nat. Mat.*, **33**, (2010).
38. M. Ménétrier, I. Saadoune, S. Levasseur, and C. Delmas, *J. Mater. Chem.*, **9**, 1135 (1999).
39. A. Van der Ven, M. K. Aydinol, G. Ceder, G. Kresse, and J. Hafner, *Phys. Rev. B*, **58**, 2975 (1998).
40. R. E. Doe, K. Persson, Y. S. Meng, and G. Ceder, *Chem. Mater.*, **20**, 5274 (2008).
41. J. S. Reed, Ph.D. Thesis "Ab-Initio Study of Cathode Materials for Lithium Batteries", pp 74, MIT, USA, 2003.